American Scientific Research Journal for Engineering, Technology, and Sciences (ASRJETS)
ISSN (Print) 2313-4410, ISSN (Online) 2313-4402

http://asrjetsjournal.org/

A Green Antisolvent Strategy for Enhancing the Performance of Carbon-based $CsPbIBr_2$ Solar Cells

Rufeng Wang[a], Haiming Zhang[b]*

[a,b]*School of Physical Science and Technology, Tiangong University, Tianjin 300387, CHN*
[a]*Email: 457755842@qq.com*
[b]*Email: zhmtjwl@163.com*

Abstract

All-inorganic $CsPbIBr_2$ perovskite materials demonstrated to own a balanceable feature for its acceptable bandgap, good phase stability and excellent thermal stability. Herein, we introduce ethyl acetate (EA) and chlorobenzene (CB) as antisolvent to improve the quality of $CsPbIBr_2$ thin films. Compared with CB, EA is a good green antisolvent, and high-quality $CsPbIBr_2$ thin films with enlarged grain sizes, few grain boundaries as well as improved optical properties were obtained by optimizing EA as antisolvent. Based on a carbon-based and hole-free planar heterojunction structure of FTO/TiO_2/$CsPbIBr_2$/Carbon, an optimal power conversion efficiency (PCE) of 4.35% was achieved, 10% enhancement in PCE. This work contributes to selecting nontoxic solvent engineering for realizing the preparation of high-quality $CsPbIBr_2$ thin films and the improved performance of all-inorganic $CsPbIBr_2$ PSCs.

Keywords: perovskite solar cells; antisolvent; carbon electrode; performance.

1. Introduction

Since first reported in 2009, perovskite solar cells (PSCs) have attracted widespread attention due to their high power conversion efficiencies (PCE) and low fabrication costs. After eleven years' rapid development, the efficiency record of organic-inorganic hybrid perovskite solar cells has reached up to 25.5%, which is almost comparable to traditional crystalline silicon cells[1]. However, in order to realize the potential commercialization applications, PSCs are still facing several challenges, mainly including the organic cations in organic-inorganic hybrid perovskite materials that have poor stability to heat, water and ultraviolet light, resulting in the decomposition of the hybrid perovskite materials and the reduction of the corresponding cells' performance[2].

---

* Corresponding author.

What's more, expensive organic hole transport layers (HTLs) and novel metal electrodes are commonly used in PSCs, which cause instability problems as well as the fabrication costs[3]. In contrast, all-inorganic perovskite materials have obvious advantages in terms of thermal stability and light stability, especially the all-inorganic $CsPbIBr_2$ perovskite, which demonstrates a balanceable feature for its acceptable bandgap, good phase stability and excellent thermal stability[4]. Therefore, the above advantages contribute to the rapid development of carbon-based and hole-free $CsPbIBr_2$ PSCs in recent years. However, the $CsPbIBr_2$ thin films deposited by the traditional solvent spin-coating method usually form poor film morphology, such as the appearance of many pinholes and small grains, which lead to the recombination of carriers in the perovskite films, thus having a negative effect on device performance[5]. To address the above problems, enormous efforts have been taken to improve $CsPbIBr_2$ films for device performance improvement, such as crystallization engineering, compositional engineering and interface engineering[6-8]. Zhu and his colleagues proposed an intermolecular exchange method to precisely control the growth and crystallinity of $CsPbIBr_2$ films, a high-performance device with a PCE of 9.16% was obtained[9]. And it was reported that Mn-doped $CsPbIBr_2$ film shows perfect crystallinity and morphology, alleviating the energy loss in hole transfer. As a result, the optimized Mn-doped $CsPbIBr_2$ PSC was boosted from 6.14% to 7.36%[10]. Liu and his colleagues introduced $SmBr_3$ to modify the interface between the electron transport layer (ETL) and $CsPbIBr_2$ perovskite layer, obtaining the improved crystallization and morphology of the $CsPbIBr_2$ perovskite layer with gradient energy band, thus reaching 30% increasement in PCE[11]. At the same time, the antisolvent assistance strategy has been confirmed useful in improving the quality of perovskite films in typical organic-inorganic hybrid PSCs as well as all-inorganic $CsPbI_3$ and $CsPbI_2Br$ PSCs[12, 13]. These works inspire the application of antisolvent assistance strategy in the $CsPbIBr_2$ PSCs[14, 15]. However, conventional antisolvents like toluene, chlorobenzene, dichloromethane are high toxic solvent, which are harmful to experimental safety and natural environment. So it is vital for reducing the use of toxic antisolvents and employing more green antisolvents to carry out scientific experiments. In this work, we introduce ethyl acetate (EA) and chlorobenzene (CB) as antisolvent to improve the quality of $CsPbIBr_2$ films through the conventional one-step solution method. Compared with CB, EA is not only a good green antisolvent with low toxicity, but also helpful for the formation of high-quality $CsPbIBr_2$ films with enlarged grain sizes, few grain boundaries, improved optical properties as well as reduced charge carrier recombination. Consequently, we obtained a champion PCE value of 4.36% based on carbon-based and hole-free $CsPbIBr_2$ PSCs, 10% enhancement in PCE. Furthermore, the devices prepared through the antisolvent assistance strategy showed good repeatability.

2. Experimental

2.1 Fabrication of solar cells

All chemicals and reagents in this work were directly used without any further purification. Firstly, the cleaned FTO conductive glass was treated under oxygen plasma for 20 min. Then, 4.5 mL pure $TiCl_4$ (Titanium tetrachloride) precursor solvent was slowly dropped into the frozen water (200 mL), accompanying with the magnetic stirring to make the solution clear and colorless. Then placing the cleaned FTO conductive glass into the solution. After 70 ℃ and 30 min reaction time, cleaning the glass with deionized water followed by annealing at 450 ℃ for 30 min, then the TiO_2 electrode transport layer (ETL) was formed. Next, 1M $CsPbIBr_2$

perovskite precursor was spinning on the TiO_2 surface at 600 rpm 5 s and 3500 rpm 40 s. During this process, 200 uL CB or EA was added into the spinning films after 20 s of beginning of the second spinning stage, respectively. Meanwhile, these substrates were annealed at 240 ℃ for 10 min. Finally, the carbon back electrode was prepared through a doctor-blade method, followed by a heat treatment at 110 ℃ for 20 min.

2.2 Characterization

The analysis of phase structure was studied by X-ray Diffraction (XRD, Bruker) with Cu Kα radiation (λ=1.5418 Å). Top-view morphologies of perovskite films were conducted by cold field emission scanning electron microscopy (SEM, Hitachi). Steady-state photoluminescence spectra (PL) were performed using a fluorescence spectrometer (Hitachi). UV-visible (UV-vis) absorption spectra were obtained with a UV-vis NIR spectrophotometer (PerkinElmer). The short-circuit current with open-circuit voltage curves (J-V curves) and external quantum efficiency (EQE) measurements of the $CsPbIBr_2$ PSCs were obtained by a simulated sunlight system (Newport) and quantum efficiency measurement system (EnliTech), respectively.

3. Results and discussion

For convenience, the $CsPbIBr_2$ films or PSCs treated by CB and EA are marked as CB-$CsPbIBr_2$ and EA-$CsPbIBr_2$, respectively. **Figure 1** presents the XRD patterns of $CsPbIBr_2$ films treated by two different antisolvents. The XRD peaks located at 14.85°, 21.10° and 30.03° correspond to the (100), (110) and (200) planes of cubic phase $CsPbIBr_2$ perovskite[16, 17]. No additional peaks appear in both two films, proving that no new phases were formed after antisolvent processes. The main peak intensities of (100) and (200) planes in EA-$CsPbIBr_2$ films are respectively higher than that of the CB-$CsPbIBr_2$ films, indicating the former has the enhanced crystallinity, which is helpful for light absorption.

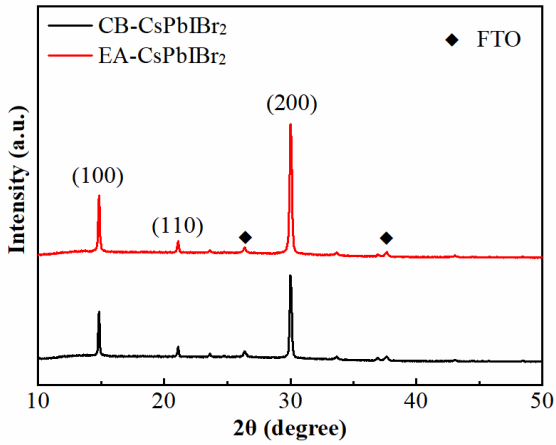

Figure 1: XRD patterns of $CsPbIBr_2$ films treated by CB and EA antisolvent.

The effect of antisolvent processes on optical properties was investigated. All CB-$CsPbIBr_2$ films and EA-$CsPbIBr_2$ films were directly deposited on insulating glass substrates. **Figure 2(a)** firstly gives the ultraviolet-visible (UV-vis) absorption spectra of CB-$CsPbIBr_2$ films and EA-$CsPbIBr_2$ films. It can be seen that both two antisolvent processes did not cause obvious changes in the absorption edge in UV−vis absorption spectra. And

the identical absorption onset at approximately 610 nm, corresponding to the bandgap of ~ 2.05 eV calculated from the Tauc plots in **Figure 2(b)**. Despite the unchanged bandgap, the EA-$CsPbIBr_2$ films showed stronger absorption compared with the CB-$CsPbIBr_2$ films, which helps to increase the light-harvest ability. In addition, the steady-state PL spectra of two different $CsPbIBr_2$ films are displayed in **Figure 2(c)**. Both the CB-$CsPbIBr_2$ films and EA-$CsPbIBr_2$ films exhibited a PL emission peak at ~ 605 nm. Notably, the PL intensity of EA-$CsPbIBr_2$ films was higher than that of CB-$CsPbIBr_2$ films, indicating the reduced nonradiative recombination process caused by defects in $CsPbIBr_2$ films, which is ascribed to the improved morphology of EA-$CsPbIBr_2$ films, such as the enlarged grain sizes with decreased grain boundaries.

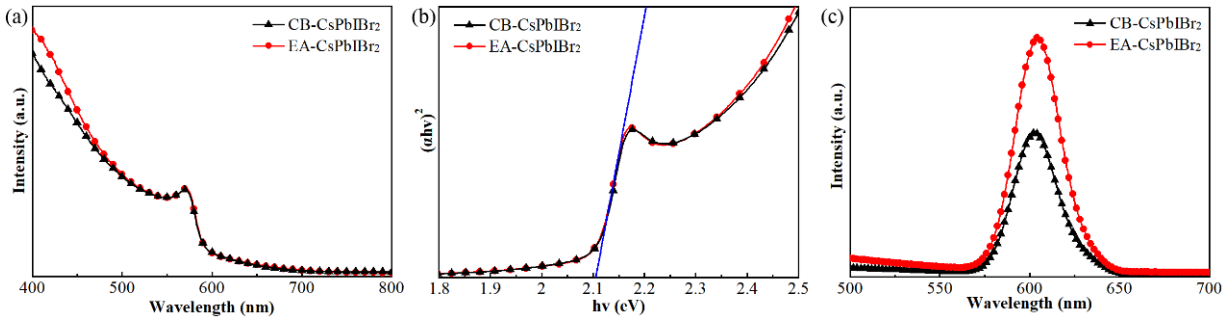

Figure 2: (a) UV−vis absorption spectra, (b) the corresponding Tauc plots calculated from the UV−vis absorption spectra and (c) steady-state PL spectra of CB-$CsPbIBr_2$ films and EA-$CsPbIBr_2$ films deposited on insulating glass substrates, respectively.

Figure 3(a-b) displays the top-view SEM images of $CsPbIBr_2$ films with two different antisolvents (CB and EA) on the TiO_2/FTO substrate. Both the CB-$CsPbIBr_2$ films and EA-$CsPbIBr_2$ films show full coverage and uniform morphology, and no obvious pinholes appeared. However, the top-view images of EA-$CsPbIBr_2$ films exhibit quite high quality with the large grain size, the detailed grain sizes of statistical charts are shown in **Figure 3(c-d)**, in which the average grain sizes were ~ 320 nm and ~ 410 nm for CB-$CsPbIBr_2$ films and EA-$CsPbIBr_2$ films, respectively. The larger grain sizes with fewer grain boundaries of the perovskite morphology help to reduce the carriers nonradiative recombination process in perovskite films, which would have a positive role in optimizing the performance of all-inorganic perovskites solar cells[18, 19].

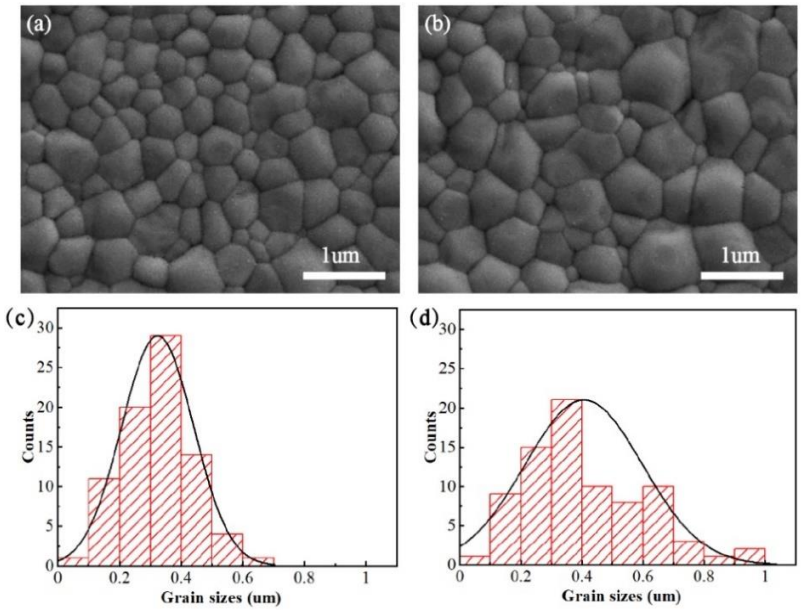

Figure 3: The top-view SEM images of (a) CB-$CsPbIBr_2$ films, (b) EA-$CsPbIBr_2$ films; (c) and (d) are the corresponding grain sizes of statistical charts for CB-$CsPbIBr_2$ films and EA-$CsPbIBr_2$ films, respectively.

In order to investigate the potential improvement of different antisolvent treatments on the photovoltaic

performance of all-inorganic $CsPbIBr_2$ PSCs, the devices with a configuration of FTO/TiO_2/$CsPbIBr_2$/Carbon was fabricated in the nitrogen glove box. **Figure 4(a)** is the schematic sketch of the carbon-based $CsPbIBr_2$ PSCs, in which the carbon electrode is used as the anode and the hole transport layer (HTL). **Figure 4(b)** gives the current-voltage curves of $CsPbIBr_2$ PSCs with two different antisolvents (CB and EA), all the detailed photovoltaic parameters such as short-circuit current (J_{sc}), open-circuit voltage (V_{oc}), fill factor (FF), and PCE, are listed in **Table 1**. The champion PCE values of the CB-$CsPbIBr_2$ PSCs and the EA-$CsPbIBr_2$ PSCs are 4.35% and 3.95% at the reverse scan directions, respectively. The improved PCE value of EA-$CsPbIBr_2$ PSCs is mainly attributed to the optimized morphology with improved grain crystallinity and enlarged grain sizes, which lead to the slight enhancement in J_{sc}, V_{oc} and FF values. Indeed, we have also investigated the EQE spectra of the CB-$CsPbIBr_2$ PSCs and the EA-$CsPbIBr_2$ PSCs, the results are shown in **Figure 4(c)**. The EA-$CsPbIBr_2$ PSC owns higher EQE values than that of the CB-$CsPbIBr_2$ PSCs within a spectral response range of 400-500 nm, indicating the enhanced light absorption ability in EA-$CsPbIBr_2$ PSCs.

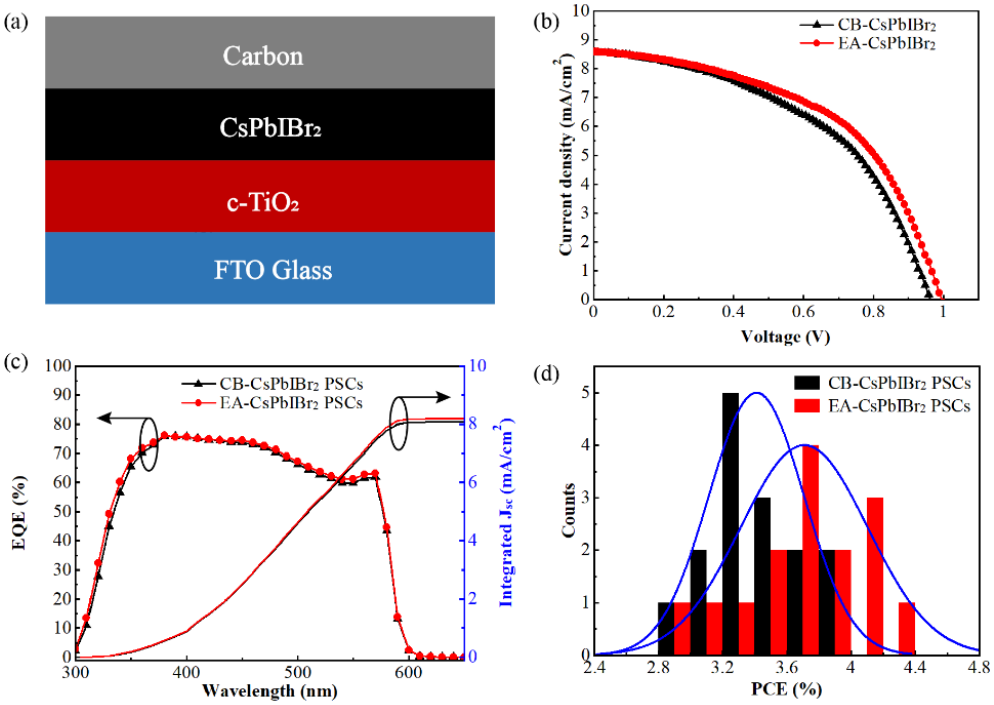

Figure 4: (a) Schematic sketch of the carbon-based $CsPbIBr_2$ PSC; (b), (c) and (d) are J-V curves, EQE spectra and PCE distribution histograms of $CsPbIBr_2$ PSCs with two different antisolvents (CB and EA), respectively.

Table 1: Photovoltaic parameters of $CsPbIBr_2$ PSCs with two antisolvents (CB and EA)

Sample	J_{sc} [mA/cm^2]	V_{oc} [V]	FF	PCE [%]
CB-$CsPbIBr_2$	8.54	0.96	0.48	3.95
EA-$CsPbIBr_2$	8.56	1.00	0.51	4.35

Besides, the integrated J_{sc} calculated from the EQE spectrum are 8.05 mA/cm^2 and 8.16 mA/cm^2 for the CB-$CsPbIBr_2$ PSCs and the EA-$CsPbIBr_2$ PSCs, respectively, which are closed to the corresponding J_{sc} values obtained in the J-V curves, implying the accuracy of the J-V measurements. Additionally, the statistical PCE distributions of $CsPbIBr_2$ PSCs with two different antisolvents (15 devices each) are compared and summarized in **Figure 4(d)**. On the one hand, both two antisolvent processes showed good repeatability; on the other hand, the average PCE value of EA-$CsPbIBr_2$ PSCs are higher than that of the CB-$CsPbIBr_2$ PSCs, which mainly ascribed to the improved $CsPbIBr_2$ films including enlarged grain sizes with fewer grain groundaries, enhanced light absorption ability as well as reduced defects.

4. Conclusion

In summary, a green antisolvent strategy was introduced to improve the quality of $CsPbIBr_2$ films. We select EA and CB as antisolvents to prepare $CsPbIBr_2$ thin films and carbon-based $CsPbIBr_2$ PSCs with a structure of FTO/c-TiO_2/$CsPbIBr_2$/Carbon. Compared with the CB-$CsPbIBr_2$ films, our results demonstrated that the EA-$CsPbIBr_2$ films exhibited an enhanced crystallinity, larger grain sizes and fewer grain boundaries, enhanced UV-

visible light absorption intensity as well as reduced carrier nonradiative recombination. Thus the corresponding EA-$CsPbIBr_2$ PSC showed improved photovoltaic parameters, the optimal efficiency reached 4.35%, which was 3.95% for the CB-$CsPbIBr_2$ PSC, an increase of 10% in PCE. At the same time, the devices prepared through antisolvent methods showed good repeatability. This work contributes to selecting nontoxic solvent engineering for realizing the preparation of high-quality $CsPbIBr_2$ thin films and the improved performance of carbon-based all-inorganic $CsPbIBr_2$ PSCs.

Acknowledgements

Thanks to professor Zhang's guidance during the whole research process.

References

[1]. X. Wu, F. Qi, F. Li, X. Deng, Z. Li, S. Wu, T. Liu, Y. Liu, J. Zhang, and Z. Zhu, "Low-Temperature Processed Carbon Electrode-Based Inorganic Perovskite Solar Cells with Enhanced Photovoltaic Performance and Stability," Energy & Environmental Materials, vol. 4, no. 1, pp. 95-102, 2021.

[2]. Y. Wu, X. Yang, W. Chen, Y. Yue, M. Cai, F. Xie, E. Bi, A. Islam, and L. Han, "Perovskite solar cells with 18.21% efficiency and area over 1 cm^2 fabricated by heterojunction engineering," Nature Energy, vol. 1, no. 11, pp. 16148, 2016.

[3]. W. Zhu, Z. Zhang, D. Chen, W. Chai, D. Chen, J. Zhang, C. Zhang, and Y. Hao, "Interfacial Voids Trigger Carbon-Based, All-Inorganic $CsPbIBr_2$ Perovskite Solar Cells with Photovoltage Exceeding 1.33 V," Nano-Micro Letters, vol. 12, no. 1, 2020.

[4]. P. Liu, X. Yang, Y. Chen, H. Xiang, W. Wang, R. Ran, W. Zhou, and Z. Shao, "Promoting the Efficiency and Stability of $CsPbIBr_2$-Based All-Inorganic Perovskite Solar Cells through a Functional Cu^{2+} Doping Strategy," ACS Applied Materials & Interfaces, vol. 12, no. 21, pp. 23984-23994, 2020.

[5]. Y. Guo, X. Yin, J. Liu, S. Wen, Y. Wu, and W. Que, "Inorganic $CsPbIBr_2$-Based Perovskite Solar Cells: Fabrication Technique Modification and Efficiency Improvement," Solar RRL, vol. 3, no. 9, pp. 1900135, 2019.

[6]. J. Lu, S.-C. Chen, and Q. Zheng, "Defect Passivation of $CsPbIBr_2$ Perovskites for High-Performance Solar Cells with Large Open-Circuit Voltage of 1.28 V," ACS Applied Energy Materials, vol. 1, no. 11, pp. 5872-5878, 2018.

[7]. W. Zhu, Z. Zhang, W. Chai, Q. Zhang, D. Chen, Z. Lin, J. Chang, J. Zhang, C. Zhang, and Y. Hao, "Band Alignment Engineering Towards High Efficiency Carbon-Based Inorganic Planar $CsPbIBr_2$ Perovskite Solar Cells," ChemSusChem, vol. 12, no. 10, pp. 2318-2325, 2019.

[8]. C. Liu, W. Li, J. Chen, J. Fan, Y. Mai, and R. E. I. Schropp, "Ultra-thin MoO_x as cathode buffer layer for the improvement of all-inorganic $CsPbIBr_2$ perovskite solar cells," Nano Energy, vol. 41, pp. 75-83, 2017.

[9]. W. Zhu, Q. Zhang, D. Chen, Z. Zhang, Z. Lin, J. Chang, J. Zhang, C. Zhang, and Y. Hao, "Intermolecular Exchange Boosts Efficiency of Air-Stable, Carbon-Based All-Inorganic Planar $CsPbIBr_2$ Perovskite Solar Cells to Over 9%," Advanced Energy Materials, vol. 8, no. 30, pp. 1802080, 2018.

[10]. J. Liang, Z. Liu, L. Qiu, Z. Hawash, L. Meng, Z. Wu, Y. Jiang, L. K. Ono, and Y. Qi, "Enhancing Optical, Electronic, Crystalline, and Morphological Properties of Cesium Lead Halide by Mn Substitution for High-Stability All-Inorganic Perovskite Solar Cells with Carbon Electrodes," Advanced Energy Materials, vol. 8, no. 20, pp. 1800504, 2018.

[11]. W. S. Subhani, K. Wang, M. Du, X. Wang, and S. Liu, "Interface-Modification-Induced Gradient Energy Band for Highly Efficient $CsPbIBr_2$ Perovskite Solar Cells," Advanced Energy Materials, vol. 9, no. 21, pp. 1803785, 2019.

[12]. N. J. Jeon, J. H. Noh, Y. C. Kim, W. S. Yang, S. Ryu, and S. I. Seok, "Solvent engineering for high-performance inorganic–organic hybrid perovskite solar cells," Nature Materials, vol. 13, no. 9, pp. 897-903, 2014.

[13]. M. Xiao, F. Huang, W. Huang, Y. Dkhissi, Y. Zhu, J. Etheridge, A. Gray-Weale, U. Bach, Y.-B. Cheng, and L. Spiccia, "A Fast Deposition-Crystallization Procedure for Highly Efficient Lead Iodide Perovskite Thin-Film Solar Cells," Angewandte Chemie International Edition, vol. 53, no. 37, pp. 9898-9903, 2014.

[14]. J. Bian, Y. Wu, W. Bi, L. Liu, X. Su, and B. Zhang, "Efficient $CsPbIBr_2$ Perovskite Solar Cells: Precise Control of Film Growth through the Application of Organic Iodized Salt and Anti-solvent," Energy & Fuels, vol. 34, no. 9, pp. 11472-11478, 2020.

[15]. B. Zhang, W. Bi, Y. Wu, C. Chen, H. Li, Z. Song, Q. Dai, L. Xu, and H. Song, "High-Performance $CsPbIBr_2$ Perovskite Solar Cells: Effectively Promoted Crystal Growth by Antisolvent and Organic Ion Strategies," ACS Applied Materials & Interfaces, vol. 11, no. 37, pp. 33868-33878, 2019.

[16]. Z. Guo, S. Teo, Z. Xu, C. Zhang, Y. Kamata, S. Hayase, and T. Ma, "Achievable high Voc of carbon based all-inorganic $CsPbIBr_2$ perovskite solar cells through interface engineering," Journal of Materials Chemistry A, vol. 7, no. 3, pp. 1227-1232, 2019.

[17]. Q. Ma, S. Huang, X. Wen, M. A. Green, and A. W. Y. Ho-Baillie, "Hole Transport Layer Free Inorganic $CsPbIBr_2$ Perovskite Solar Cell by Dual Source Thermal Evaporation," Advanced Energy Materials, vol. 6, no. 7, 2016.

[18]. H. Sun, J. Zhang, X. Gan, L. Yu, H. Yuan, M. Shang, C. Lu, D. Hou, Z. Hu, Y. Zhu, and L. Han, "Pb- Reduced $CsPb_{0.9}Zn_{0.1}$ I_2Br Thin Films for Efficient Perovskite Solar Cells," Advanced Energy Materials, vol. 9, no. 25, 2019.

[19]. S.-H. Chan, M.-C. Wu, K.-M. Lee, W.-C. Chen, T.-H. Lin, and W.-F. Su, "Enhancing perovskite solar cell performance and stability by doping barium in methylammonium lead halide," Journal of Materials Chemistry A, vol. 5, no. 34, pp. 18044-18052, 2017.